

One-loop radiative corrections to photon-pair production in polarized positron-electron annihilation

S. Bondarenko¹, Ya. Dydyshka^{2,3}, L. Kalinovskaya², A. Kampf²,
L. Rumyantsev², R. Sadykov², and V. Yermolchuk^{2,3}

¹Bogoliubov Laboratory of Theoretical Physics, JINR, 141980 Dubna, Moscow region, Russia

²Dzhelepov Laboratory of Nuclear Problems, JINR, 141980 Dubna, Moscow region, Russia

³Institute for Nuclear Problems, Belarusian State University, Minsk, 220006 Belarus

November 22, 2022

Abstract

A theoretical description of photon-pair production in polarized positron-electron annihilation is presented. Complete one-loop electroweak radiative corrections are calculated taking into account the exact dependence on the electron mass. Analytical results are derived with the help of the **SANC** system. The relevant contributions to the cross section are calculated analytically using the helicity amplitude approach. The cases of unpolarized and longitudinally polarized fermions in the initial state are investigated. Calculations are realized in the Monte Carlo integrator **MCSANCe** and generator **ReneSANCe** which allow one the implementation of any experimental cuts used in the analysis of e^+e^- annihilation data of both low and high energies.

1 Introduction

The comprehensive long-term program of next generation e^+e^- colliders proposes a large potential improvement in ultra-precise measurements of electroweak (EW) parameters and the creation of modern tools for adequate luminosity estimates. Future e^+e^- colliders such as **FCC-ee** [1], **ILC** [2], **CEPC** [3,4] and **CLIC** [5] will have a total luminosity 2-3 orders of magnitude larger than the LEP total luminosity and the possibility of using polarizing beams that could provide an additional probe of the accuracy test of the Standard model as well as in the search for new physics. The determination of the luminosity at lepton colliders is a necessary task, since the normalization of measured cross sections is an observable quantity of immediate phenomenological interest. Per mille precision of the integrated luminosity measurement at future colliders seems feasible in terms of existing technologies [6].

In practice, this problem is solved by choosing three specific reference processes which generate large statistics, are as free as possible from systematic ambiguities, and are predicted by theory with suitable accuracy: small and large angle Bhabha scattering, lepton-pair production in e^+e^- collisions and large angle e^+e^- annihilation to photon pair.

The main result of this work is the independent calculation of the complete one-loop EW radiative corrections (RCs) taking into account the exact dependence of the e^+e^- annihilation to photon pair on the electron mass

$$e^+(p_1, \chi_1) + e^-(p_2, \chi_2) \rightarrow \gamma(p_3, \chi_3) + \gamma(p_4, \chi_4) (+\gamma(p_5, \chi_5)), \quad (1)$$

and arbitrary longitudinal polarization of initial particles. Here p_i are the 4-momenta and χ_i are the helicities of the corresponding particles.

The photon-pair production plays a central role in the determination of the luminosity for the following reasons: events have two collinear photons at large angles providing a clean signature; the theoretical accuracy for the Bhabha process and the s-channel is limited by an uncertainty in the hadronic contribution $\Delta\alpha_5^{hadr}(s)$ to the vacuum polarization $\Pi_{\gamma\gamma}$, but in the case of the process under consideration the hadronic contribution to the vacuum polarization enters only at the two-loop level and the theoretical accuracy of $\Delta\alpha_5^{hadr}(s)$ is approximately of an order of 10^{-6} [7].

Process (1) was first investigated in the classical papers [8], [9], and later in [10]. Now it has already been studied at the one-loop level in connection with experiments at future e^+e^- colliders. For the first time this was done in [10]. Modern Monte-Carlo tools for the process (1) are MC generators **MCGPJ** [11] and **BabaYaga@NLO** [7, 12–14]. The recent version of the MC **BabaYaga@NLO** contains one-loop calculations and also provides an enhancement of leading logarithmic (LL) QED contributions due to multiphoton emission and the impact of photonic and fermion-loop corrections at next-to-next-to-leading order [7].

In the present paper, the calculations in the framework of **SANC** are carried out at the one-loop level within the OMS (on-mass-shell) renormalization scheme in R_ξ and in the unitary gauge as a cross-check. Loop integrals are expressed in terms of the standard scalar Passarino-Veltman functions [15]. To parameterize the ultraviolet divergences, dimensional regularization was used. Numerical results were obtained by the MC generator **ReneSANCe** [16] and integrator **MCSANCee**. To date, theoretical uncertainties by **SANC** have been investigated for the complete one-loop and leading higher-order EW corrections and with taking into account polarization in the initial and final states for the following processes: Bhabha scattering [17], e^+e^- annihilation to ZH and $Z\gamma$ [18], s-channel [19], Møller scattering [20], and polarized μe scattering [21].

This article consists of four Sections. We describe the methodology of calculations of polarized cross sections at the complete one-loop EW level in the massive basis within the helicity approach in Section 2. The evaluation of theoretical uncertainties for unpolarized **FCCee**, **CEPC** and polarized **ILC**, **CLIC** future experiments and the results of a comprehensive comparison of the independent MC codes for cross-checking are presented in Section 3. Summary is drawn in Section 4.

2 Differential cross section

The cross section of the process of the longitudinally polarized positron e^+ and electron e^- beams with the polarization degrees P_e^+ and P_e^- , respectively, can be written as follows:

$$\sigma(P_{e^+}, P_{e^-}) = \frac{1}{4} \sum_{\chi_1, \chi_2} (1 + \chi_1 P_{e^+})(1 + \chi_2 P_{e^-}) \sigma_{\chi_1 \chi_2}, \quad (2)$$

where $\chi_{1(2)} = -1(+1)$ correspond to the particle i with the left (right) helicity.

The complete one-loop cross section of the process can be split into four parts

$$\sigma^{\text{one-loop}} = \sigma^{\text{Born}} + \sigma^{\text{virt}}(\lambda) + \sigma^{\text{soft}}(\lambda, \omega) + \sigma^{\text{hard}}(\omega). \quad (3)$$

Here σ^{Born} is the Born cross section, σ^{virt} is the contribution of virtual (loop) corrections, $\sigma^{\text{soft(hard)}}$ is the soft (hard) photon emission contribution (the hard photon energy $E_\gamma > \omega$). The auxiliary parameters λ ("photon mass") and ω are canceled after summation. Note that in calculations of one-loop RCs we can separate QED and pure weak interaction effects.

We apply the HA approach to all four components of the one-loop cross sections.

The virtual (Born) cross section of the $e^+ + e^- \rightarrow \gamma + \gamma$ process has the following form:

$$\frac{d\sigma_{\chi_1 \chi_2}^{\text{virt(Born)}}}{d \cos \vartheta} = \pi \alpha^2 \frac{1}{4\beta_e} |\mathcal{H}_{\chi_1 \chi_2}^{\text{virt(Born)}}|^2, \quad (4)$$

where $\beta_e = \sqrt{1 - 4m_e^2/s}$, ϑ is the angle between the p_1 and p_3 and

$$|\mathcal{H}_{\chi_1 \chi_2}^{\text{virt(Born)}}|^2 = \sum_{\chi_3, \chi_4} |\mathcal{H}_{\chi_1 \chi_2 \chi_3 \chi_4}^{\text{virt(Born)}}|^2. \quad (5)$$

The cross section for the hard photon bremsstrahlung is given by the expression

$$\frac{d\sigma_{\chi_1 \chi_2}^{\text{hard}}}{ds' d \cos \vartheta_3 d \phi_3 d \cos \vartheta_5} = \alpha^3 \frac{s - s'}{192\pi s^2 \beta_e} |\mathcal{H}_{\chi_1 \chi_2}^{\text{hard}}|^2, \quad (6)$$

where $s' = (p_3 + p_4)^2$ and

$$|\mathcal{H}_{\chi_1 \chi_2}^{\text{hard}}|^2 = \sum_{\chi_3, \chi_4, \chi_5} |\mathcal{H}_{\chi_1 \chi_2 \chi_3 \chi_4 \chi_5}^{\text{hard}}|^2. \quad (7)$$

Here ϑ_5 is the angle between p_1 and p_5 in the laboratory frame, ϑ_3 is the angle between 3-momenta p_3 and p_5 in the rest frame of $(p_3 p_4)$ -compound, ϕ_3 is the azimuthal angle of the p_3 in the rest frame of $(p_3 p_4)$ -compound.

2.1 The Born and virtual contributions

The first step is the calculation of the Covariant Amplitude (CA) and form factors (\mathcal{F}_i). In the system **SANC** we calculate the CA of the annihilation to vacuum, i.e. $2f2b \rightarrow 0$, and then turn over to the selected channel. Then the helicity amplitudes (HAs) will be constructed.

2.1.1 Covariant amplitude for the Born and virtual parts

The covariant one-loop amplitude corresponds to the result of the straightforward standard calculation of all diagrams contributing to a given process at the tree (Born) and one-loop levels. The CA is represented in a certain basis made of strings of Dirac matrices and/or external momenta (structures) contracted with polarization vectors of bosons $\varepsilon(p_i)$. The CA can be written in an explicit form using scalar form factors \mathcal{F}_i . All masses, kinematic invariants and coupling constants, and other parameter dependencies are included into these form factors, but tensor structures with Lorenz indices made from strings of Dirac matrices are given by the basis.

Using the multichannel approach, we have found a complete massive basis and covariant amplitude. The covariant amplitude for the processes we are interested in can be obtained from Eq. (8) by exploiting crossing symmetry. We found 40 structures for the CA. By applying algebraic transformations, we simplified the number of structures down to 24. Using photon transversality, we obtained 6 ratios for vector and 5 for axial form factors \mathcal{F}_i . The final answer for the basis is 8 structures for the tensor and 4 structures for the pseudotensor. In accordance with this, the next-to-leading order (NLO) EW RCs to the process $2f2\gamma \rightarrow 0$ can be parameterized in terms of 14 scalar form factors and the corresponding basic matrix elements, 8 vector and 4 axial ones.

For the covariant amplitude we have:

$$\begin{aligned} \mathcal{A}_{l+l-\gamma\gamma} = & \bar{v}(p_1) \left[\text{Str}_{\mu\nu}^{v,0} (v_f \mathcal{F}^{0,v}(s, t, u)) + \sum_{j=1}^7 \text{Str}_{\mu\nu}^{v,j} \mathcal{F}^{j,v}(s, t, u) \right. \\ & \left. + \sum_{i=1}^4 \text{Str}_{\mu\nu}^{a,i} \gamma_5 \mathcal{F}^{i,a}(s, t, u) \right] u(p_2) \varepsilon_\nu^\gamma(p_3) \varepsilon_\mu^\gamma(p_4), \end{aligned} \quad (8)$$

with the structures

$$\begin{aligned}
\text{Str}_{\mu\nu}^{v,0} &= \frac{s}{(m_l^2 - t)(m_l^2 - u)} \left[-(iK_2 + m_l)\tau_{\mu\nu}^6 + 2i\frac{1}{m_l^2 - u} \left(\tau_{\mu\nu}^7 - \tau_{\mu\nu}^9 - \frac{1}{2}(\not{p}_3 - \not{p}_4)\tau_{\mu\nu}^{10} \right) \right], \\
\text{Str}_{\mu\nu}^{v,1} &= iK_2 \left(\frac{2}{s}\tau_{\mu\nu}^3 + \tau_{\mu\nu}^{10} \right), \\
\text{Str}_{\mu\nu}^{v,2} &= -i \left(K_2(k_t^2\tau_{\mu\nu}^3 - \tau_{\mu\nu}^4) + \frac{1}{2}k_t [\tau_{\mu\nu}^1 + 2im_l(\tau_{\mu\nu}^5 + sk_t\tau_{\mu\nu}^{10})] \right), \\
\text{Str}_{\mu\nu}^{v,3} &= i \left[\frac{1}{2}\tau_{\mu\nu}^1 + 2K_2k_t\tau_{\mu\nu}^3 + (-K_2 + im_l)\tau_{\mu\nu}^5 + im_lsk_t\tau_{\mu\nu}^{10} \right], \\
\text{Str}_{\mu\nu}^{v,4} &= \frac{4im_l}{s}K_2\tau_{\mu\nu}^3 + \frac{s}{2}\tau_{\mu\nu}^6 + \not{p}_4\tau_{\mu\nu}^7 - \not{p}_3\tau_{\mu\nu}^9 - (m_l^2 + t)\tau_{\mu\nu}^{10}, \\
\text{Str}_{\mu\nu}^{v,5} &= -\tau_{\mu\nu}^0 - \frac{2}{s}im_l\tau_{\mu\nu}^1 - \frac{1}{2}(m_l^2 - t)\tau_{\mu\nu}^6 - 2k_t \left[\frac{2}{s}im_lK_2\tau_{\mu\nu}^3 - \tau_{\mu\nu}^5 - \frac{(3m_l^2 - t)}{2}\tau_{\mu\nu}^{10} \right], \\
\text{Str}_{\mu\nu}^{v,6} &= \frac{s}{2} \left(\frac{2}{s}\tau_{\mu\nu}^3 + \tau_{\mu\nu}^{10} \right), \\
\text{Str}_{\mu\nu}^{v,7} &= \tau_{\mu\nu}^4 - k_t \left(\tau_{\mu\nu}^5 + \frac{m_l^2 - t}{2}\tau_{\mu\nu}^{10} \right), \\
\text{Str}_{\mu\nu}^{a,1} &= -i \left(K_2\tau_{\mu\nu}^6 + \frac{4}{s}k_tK_2\tau_{\mu\nu}^3 - \left(k_t - i\frac{2m_l}{s}\not{p}_4 \right) \tau_{\mu\nu}^7 + (k_t + im_l\not{p}_3) \tau_{\mu\nu}^9 \right), \\
\text{Str}_{\mu\nu}^{a,2} &= iK_2 \left(\frac{2}{s}\tau_{\mu\nu}^3 + \tau_{\mu\nu}^{10} \right), \\
\text{Str}_{\mu\nu}^{a,3} &= -\frac{1}{2}\tau_{\mu\nu}^2 - iK_2(k_t^2\tau_{\mu\nu}^3 - \tau_{\mu\nu}^4), \\
\text{Str}_{\mu\nu}^{a,4} &= -\frac{1}{2}\tau_{\mu\nu}^2 + iK_2k_t(2k_t\tau_{\mu\nu}^3 + \tau_{\mu\nu}^5). \tag{9}
\end{aligned}$$

where $\bar{v}(p_1)$, $u(p_2)$ and m_e are the bispinors and the mass of the external fermions, respectively; $\varepsilon_\nu^\gamma(p_3)$ and $\varepsilon_\mu^\gamma(p_4)$ denote the photon polarization vector; the vector and axial gauge-boson-to-fermion couplings are denoted by v_l and a_l , respectively; $\mathcal{F}^{j,v}$ and $\mathcal{F}^{i,a}$ stand for the scalar form factors, where $\mathcal{F}^{0,v}$ and $\text{Str}_{\mu\nu}^0$ correspond to the lowest-order matrix element and

$$K_2 = \frac{1}{2}(\not{p}_3 - \not{p}_4 + \not{p}_2 - \not{p}_1).$$

To obtain a compact form of the amplitude structures, we choose 10 auxiliary strings

$$\begin{aligned}
\tau_{\mu\nu}^0 &= \gamma^\mu \not{p}_3 p_2^\nu + \not{p}_4 \gamma^\nu p_1^\mu, \\
\tau_{\mu\nu}^1 &= s \left[\gamma^\nu (k_u p_1^\mu - k_t(p_2^\mu - p_4^\mu)) - \gamma^\mu (k_u p_2^\nu - k_t(p_1^\nu - p_3^\nu)) \right], \\
\tau_{\mu\nu}^2 &= (m_l K_2 - it) [\gamma^\nu (p_1^\mu + k_t p_3^\mu) + \gamma^\mu (p_2^\nu + k_t p_4^\nu)], \\
\tau_{\mu\nu}^3 &= p_3^\mu p_4^\nu, \tau_{\mu\nu}^4 = p_1^\mu p_2^\nu, \tau_{\mu\nu}^5 = p_1^\mu p_4^\nu + p_2^\nu p_3^\mu, \\
\tau_{\mu\nu}^6 &= \gamma^\mu \gamma^\nu, \tau_{\mu\nu}^7 = \gamma^\nu p_3^\mu, \tau_{\mu\nu}^8 = \gamma^\mu p_4^\nu, \tau_{\mu\nu}^{10} = \delta^{\mu\nu}. \tag{10}
\end{aligned}$$

where $k_I = \frac{m_l^2 - I}{s}$, with $I = t, u$ (usual Mandelstam invariants).

In Eq. (8), we keep the fermion mass in order to maintain photon transversality without mass approximation. Moreover, in the mass-containing denominators of $\text{Str}_{\mu\nu}^0$, the mass cannot be neglected because these denominators correspond to the propagators of fermions that emit external photons and thus lead to mass singularities.

The basic matrix elements, $\text{Str}_{\mu\nu}^j$, are chosen to be explicitly transversal in the photonic 4-momentum. That is, for all of them the following relations hold:

$$\text{Str}_{\mu\nu}^j(p_3)_\nu = 0 \text{ and } \text{Str}_{\mu\nu}^j(p_4)_\mu = 0. \quad (11)$$

We have checked that the form factors $\mathcal{F}^{j,v}$ and $\mathcal{F}^{i,a}$ are free of gauge parameters and ultraviolet singularities; all calculations are made in the R_ξ gauge. The analytical expressions of the form factors are too cumbersome to be presented in this paper.

2.1.2 Helicity amplitudes for the Born and virtual parts

Using C, P, Bose and the transition between the final and initial symmetries, we write down four sets of HAs. The presence of the electron masses gives additional terms proportional to the factor m_l , which can be considered significant in calculations at low energy.

$$\begin{aligned} 1) \mathcal{H}_{++++} &= -\mathcal{H}_{----+}(A=1), \quad \mathcal{H}_{+++-} = -\mathcal{H}_{----+}(A=-1), \\ \mathcal{H}_{--+-} &= \mathcal{H}_{----+}(A=-1), \\ \mathcal{H}_{----+} &= -\frac{\sqrt{s}}{8} c^+ c^- \left\{ sm_l \cos \vartheta \mathcal{F}_{v_3} \right. \\ &\quad \left. + \sqrt{\lambda_{ee}} \left[m_l \left(\frac{8}{z_{13} z_{14}} \mathcal{F}_{v_1} + \mathcal{F}_{v_3} - 4\mathcal{F}_{v_4} \right) - 2\mathcal{F}_{v_6} + \mathcal{F}_{v_8} - Am_l (\mathcal{F}_{a_3} + \mathcal{F}_{a_4}) \right] \right\}. \end{aligned} \quad (12)$$

$$\begin{aligned} 2) \mathcal{H}_{-+ \pm \pm} &= \mathcal{H}_{-+ --}(A=1), \quad \mathcal{H}_{+- \pm \pm} = \mathcal{H}_{-+ --}(A=-1), \\ \mathcal{H}_{-+ --} &= \frac{1}{2} \sin \vartheta \left\{ s \left(\mathcal{F}_{v_2} - \frac{s}{8} (1 + \cos^2 \vartheta_{13}) \mathcal{F}_{v_3} + A \cos \vartheta \left[(\mathcal{F}_{a_1} + \frac{s}{4} (\mathcal{F}_{a_3} + \mathcal{F}_{a_4})) \right] \right) \right. \\ &\quad - \sqrt{\lambda_{ee}} \left[s \cos \vartheta \left(\frac{1}{4} \mathcal{F}_{v_3} - \frac{1}{2} \mathcal{F}_{v_4} + \frac{m_l}{s} \mathcal{F}_{v_6} \right) \right. \\ &\quad \left. \left. - A \left(\mathcal{F}_{a_1} - \mathcal{F}_{a_2} + \frac{s}{8} [(1 + \cos^2 \vartheta_{13}) \mathcal{F}_{a_3} + 2 \cos^2 \vartheta_{13} \mathcal{F}_{a_4}] \right) \right] \right\}. \end{aligned} \quad (13)$$

$$3) \mathcal{H}_{+---} = \mathcal{H}_{-++-}(A = -1), \quad (14)$$

$$\mathcal{H}_{-++-} = \mathcal{H}_{-++-}(A = 1, c^- \rightarrow -c^+), \mathcal{H}_{+--+} = \mathcal{H}_{-++-}(A = -1, c^- \rightarrow -c^+),$$

$$\begin{aligned} \mathcal{H}_{-++-} &= \frac{1}{8} \sin \vartheta s c^- \left\{ s \left[\frac{1}{2} c^- \mathcal{F}_{v3} + A \left(\frac{4}{s} \mathcal{F}_{a1} + \mathcal{F}_{a3} + \mathcal{F}_{a4} \right) \right] \right. \\ &\quad \left. - \sqrt{\lambda_{ee}} \left(\frac{4}{z_{13} z_{14}} \mathcal{F}_{v1} + \mathcal{F}_{v3} - 2\mathcal{F}_{v4} + \frac{4m_l}{s} \mathcal{F}_{v6} + A \left(\frac{1}{2} c^- \mathcal{F}_{a3} - \cos \vartheta \mathcal{F}_{a4} \right) \right) \right\}. \end{aligned}$$

$$4) \mathcal{H}_{-----} = -\mathcal{H}_{++++}(V = 1), \quad \mathcal{H}_{-++-} = -\mathcal{H}_{++++}(c^- \leftrightarrow c^+, V = -1), \quad (15)$$

$$\mathcal{H}_{+--+} = \mathcal{H}_{++++}(c^- \leftrightarrow c^+, V = -1),$$

$$\begin{aligned} \mathcal{H}_{++++} &= -\frac{\sqrt{s}}{8} \left\{ s \left[V \left(\frac{8m_l}{z_{13} z_{14}} \mathcal{F}_{v1} - 2c^+ \mathcal{F}_{v6} \right) \right. \right. \\ &\quad \left. \left. + \cos \vartheta \left(m_l \left[\frac{8}{s} \mathcal{F}_{v2} - (4 - c^+ c^-) \mathcal{F}_{v3} + 4\mathcal{F}_{v4} \right] - 4\mathcal{F}_{v5} + 2\mathcal{F}_{v8} \right) \right] \right. \\ &\quad \left. + \sqrt{\lambda_{ee}} \left[m_l \left(\frac{8}{z_{13} z_{14}} \mathcal{F}_{v1} + \frac{8}{s} \mathcal{F}_{v2} - (4 - 3c^+ c^-) \mathcal{F}_{v3} + 4 \cos^2 \vartheta_{13} \mathcal{F}_{v4} \right) \right. \right. \\ &\quad \left. \left. - 4(1 + c^-) \mathcal{F}_{v5} - 2c^+ \mathcal{F}_{v6} - 4\mathcal{F}_{v7} + 2\mathcal{F}_{v8} \right] \right\}, \end{aligned}$$

where $c^\pm = 1 \pm \cos \vartheta$.

2.2 Real photon emission corrections

The real corrections consist of soft and hard radiative contributions. They are calculated using the bremsstrahlung modules. The soft bremsstrahlung has Born-like kinematics, while the phase space of hard radiation has an extra particle, photon.

2.2.1 Soft photon bremsstrahlung

The soft photon contribution contains infrared divergences and has to compensate the corresponding divergences of one-loop virtual QED corrections. It is factorized in front of the Born cross section. It depends on the auxiliary parameter which separates the kinematic domains of the soft and hard photon emission in a given reference frame. The polarization dependence is contained in σ^{Born} .

The explicit form is

$$\sigma^{\text{soft}} = -N \sigma^{\text{Born}} \frac{2}{\beta_e} \left\{ 2 [\beta_e - k \ln x^2] \ln \frac{2\bar{\omega}}{\lambda} - \ln x + k [\ln^2 x + \text{Li}_2(1 - 1/x^2)] \right\},$$

where

$$N = \frac{\alpha}{2\pi} Q_e^2, \quad r_s = \frac{m_l}{s}, \quad k = 1 - 2r_s, \quad x = \frac{1}{\sqrt{r_s}} \frac{1 + \beta_e}{2}.$$

Here $\bar{\omega}$ is the soft-hard separator, λ is an auxiliary infinitesimal photon mass, and $L_s = \ln \frac{s}{m_e^2} - 1$.

2.2.2 Hard photon bremsstrahlung

Spin effects of hard photon bremsstrahlung for photon-pair production using the method of helicity amplitudes were investigated in [22], [23]. In the presented results, we used our universal massive module for hard photon bremsstrahlung for $l^+l^-\gamma\gamma\gamma \rightarrow 0$ by appropriately unfolding it in channel (1), where 0 stands for *vacuum*, and all masses are not neglected.

The field strength bivector is an antisymmetric tensor and can naturally be expressed as an element of the Clifford algebra of Dirac matrices by contracting with $\gamma^{[\mu}\gamma^{\nu]} = \gamma^\mu \wedge \gamma^\nu$.

Let us consider a photon with 4-momentum $k^2 = 0$ and polarization vector ε . The Maxwell bivector (contracted with Dirac matrices) is

$$\mathbf{F} \equiv F_{\mu\nu}\gamma^\mu\gamma^\nu = \not{k} \wedge \not{\varepsilon}.$$

The Maxwell equation becomes $\not{k}\mathbf{F} = 0$. It is also evident that gauge transformation $\varepsilon \rightarrow \varepsilon + Ck$ leaves the bivector \mathbf{F} unaffected.

The axial gauge can be defined by the additional condition $\varepsilon \cdot g = 0$ with some (massive) vector g . Solving it together with $\varepsilon \cdot k = 0$, we obtain a polarization vector in the axial gauge

$$\not{\varepsilon} = \frac{\not{g}\mathbf{F}\not{g}_1}{g \cdot k}, \quad \not{A}\not{g}_1 \equiv \overline{\text{Tr}}[A\gamma^\mu]\gamma_\mu, \quad \not{\varepsilon}(g_1) - \not{\varepsilon}(g_2) = -\frac{\overline{\text{Tr}}[\not{g}_1\not{g}_2\mathbf{F}]}{(g_1 \cdot k)(g_2 \cdot k)}\not{k}, \quad \overline{\text{Tr}} = \frac{1}{4}\text{Tr}.$$

Changing the vector g leads to gauge transformation.

The helicity amplitude for hard photon bremsstrahlung is organized as a sum of three cyclically symmetric terms

$$\mathcal{A} = 2\sqrt{2}(\mathcal{A}^3 + \mathcal{A}^4 + \mathcal{A}^5), \quad \mathcal{A}_3 = \mathcal{A}_5|_{5 \rightarrow 3 \rightarrow 4 \rightarrow 5}, \mathcal{A}_4 = \mathcal{A}_5|_{5 \rightarrow 4 \rightarrow 3 \rightarrow 5}.$$

So it is enough to consider only the single term. The Maxwell bivector for helicity states can be factorized $\mathbf{F}_5^{\chi_5} = u_5^{\chi_5} \bar{v}_5^{\chi_5}$, and the corresponding term decays into building blocks:

$$\begin{aligned} \mathcal{A}_{\xi_1\xi_2\chi_3\chi_4\chi_5}^5 &= R_{\xi_1}^{\chi_1}(1)R_{\xi_2}^{\chi_2}(2) \frac{-\mathcal{S}_{\chi_5}^5 \mathcal{B}_{\chi_1\chi_2\chi_3\chi_4} + \mathcal{C}_{\chi_1\chi_5}^5 \mathcal{G}_{\chi_5\chi_2\chi_3\chi_4}^5}{z_{23}z_{24}}, \\ \mathcal{S}_{\chi_5}^5 &= \frac{\text{Tr}[\not{p}_1\not{p}_2\mathbf{F}_5]}{\sqrt{2}z_{15}z_{25}}, & \mathcal{B}_{\chi_1\chi_2\chi_3\chi_4}^5 &= \bar{v}_1 \left(\not{A}_{\not{p}_2\not{p}_1} \not{F}_4 \not{A}_{\not{p}_1} - \not{p}_2 \not{A}_{\not{p}_1\not{p}_2} \not{F}_3 \not{A}_{\not{p}_2} \right) u_2, \\ \mathcal{C}_{\chi_1\chi_5}^5 &= \frac{\bar{v}_1 u_5}{z_{15}}, & \mathcal{G}_{\chi_5\chi_2\chi_3\chi_4}^5 &= \bar{v}_5 \left(\not{A}_{\not{p}_2\not{p}_1} \not{F}_4 \not{A}_{\not{p}_1} - \not{p}_2 \not{A}_{\not{p}_1\not{p}_2} \not{F}_3 \not{A}_{\not{p}_2} \right) u_2, \end{aligned}$$

with the abbreviations $u_i \equiv u^{\chi_i}(p_i)$, $\bar{v}_i \equiv \bar{v}^{\chi_i}(p_i)$, $\mathbf{F}_j \equiv \mathbf{F}^{\chi_j}(p_j)$, and $\not{A}_{\not{p}_0\not{p}_4} = \overline{\text{Tr}}[A] + \overline{\text{Tr}}[A\gamma_5]\gamma_5$.

We work in the chiral representation of gamma-matrices and exploit Weyl spinors. To decompose the Dirac spinors into Weyl components, we use the following notation:

$$\not{p} = \begin{pmatrix} \hat{p} & \check{p} \end{pmatrix}, \quad u = \begin{pmatrix} |u\rangle \\ |u] \end{pmatrix}, \quad \mathbf{F} = \begin{pmatrix} \check{\mathbf{F}} & \\ & \hat{\mathbf{F}} \end{pmatrix}, \quad \bar{v} = \left(\langle \bar{v}|, \quad [\bar{v}] \right),$$

For the massless particle with momentum p_i , we have $\check{p}_i = |i\rangle[i|$, $\hat{p}_i = |i]\langle i|$. For the massive particle with $p_i^2 = m_i^2$, we use the projection on the light-cone of some auxiliary momentum. To evaluate the term \mathcal{A}^5 of the amplitude, we find that one of the most economical choices is to use p_5 :

$$\hat{k}_i = \frac{\hat{p}_i \check{p}_5 \hat{p}_i}{2p_i \cdot p_5}, \quad \hat{k}_i = |i]\langle i|, \quad |i\rangle = \frac{\check{p}_i |5\rangle}{[i|5]}, \quad |i] = \frac{\hat{p}_i |5\rangle}{\langle i|5\rangle}$$

The Dirac solutions in terms of spinors for k_i are

$$u_i^+ = \begin{bmatrix} |i\rangle \\ m_i \\ [i|5] |5\rangle \end{bmatrix}, \quad u_i^- = \begin{bmatrix} \frac{m_i}{\langle i|5\rangle} |5\rangle \\ |i] \\ |i] \end{bmatrix}, \quad \bar{v}_i^+ = \begin{bmatrix} \langle i|, & -\frac{m_i}{[i|5]} |5] \end{bmatrix}, \quad \bar{v}_i^- = \begin{bmatrix} -\frac{m_i}{\langle i|5\rangle} \langle 5|, & [i| \end{bmatrix}$$

The explicit expressions of the amplitude components \mathcal{A} are written as follows:

$$\mathcal{B}_{\chi_1 \chi_2 \chi_3 \chi_4}^5 = \left[\begin{array}{c} m[\bar{v}_1|u_2] \langle 3|4\rangle^2 \\ [3|p_2|4] ([\bar{v}_1|3] \langle 4|u_2\rangle + \langle \bar{v}_1|4] [3|u_2]) \end{array} \quad \frac{\langle 3|p_2|4] (\langle \bar{v}_1|3] [4|u_2] + [\bar{v}_1|4] \langle 3|u_2\rangle)}{m \langle \bar{v}_1|u_2\rangle [4|3]^2} \right]_{\chi_3 \chi_4},$$

$$\mathcal{G}_{\chi_5 \chi_2 \chi_3 \chi_4}^5 = \left[\begin{array}{c} m[\bar{v}_5|u_2] \langle 3|4\rangle^2 \\ [3|p_2|4] ([\bar{v}_5|3] \langle 4|u_2\rangle + \langle \bar{v}_5|4] [3|u_2]) \end{array} \quad \frac{\langle 3|p_2|4] (\langle \bar{v}_5|3] [4|u_2] + [\bar{v}_5|4] \langle 3|u_2\rangle)}{m \langle \bar{v}_5|u_2\rangle [4|3]^2} \right]_{\chi_3 \chi_4},$$

$$\mathcal{S}_{\chi_5}^5 = \left[-\frac{[1|2]}{[1|5][2|5]} \quad -\frac{\langle 1|2\rangle}{\langle 1|5\rangle \langle 2|5\rangle} \right]_{\chi_5}, \quad \mathcal{C}_{\chi_1, \chi_5}^5 = \frac{1}{z_{15}} \begin{bmatrix} \langle 1|5\rangle & 0 \\ 0 & [1|5] \end{bmatrix}_{\chi_1 \chi_5},$$

$$\langle \bar{v}_i|u_j\rangle = \begin{bmatrix} \langle i|j\rangle & m_j \frac{\langle i|5\rangle}{\langle j|5\rangle} \\ m_i \frac{\langle 5|j\rangle}{\langle 5|i\rangle} & 0 \end{bmatrix}_{\chi_i \chi_j}, \quad [\bar{v}_i|u_j] = \begin{bmatrix} 0 & m_i \frac{[j|5]}{[i|5]} \\ m_j \frac{[5|i]}{[5|j]} & [i|j] \end{bmatrix}_{\chi_i \chi_j}.$$

From the momentum $p_i = \{E_i, p_i^x, p_i^y, p_i^z\}$ with $p_i^2 = m_i^2$ there can be built two massless vectors $k_{i^*} = \{|\vec{p}_i|, -p_i^x, -p_i^y, -p_i^z\}$ and $k_{i^b} = p_i - \frac{m_i^2}{2p_i \cdot k_{i^*}} k_{i^*}$, with $k_{i^*}^2 = k_{i^b}^2 = 0$. The corresponding spinors $|i^*\rangle$ and $|i^b\rangle$ allow evaluating the rotation matrix

$$R_{\xi_i}^{\chi_i}(i) = \begin{bmatrix} \frac{[i^b|5]}{[i|5]} & \frac{m_i \langle i^*|5\rangle}{\langle i^*|i^b\rangle \langle i|5\rangle} \\ m_i \frac{[i^*|5]}{[i^*|i^b][i|5]} & \frac{\langle i^b|5\rangle}{\langle i|5\rangle} \end{bmatrix}.$$

3 Numerical results

In this section, we firstly present comparison of the result obtained by means of the **SANC** system with the tree-level results for Born and hard photon bremsstrahlung of the **CalcHEP** [24] and **WHIZARD** [25–27] codes. Also, the NLO QED RCs are compared with the **BabaYaga** code [28] and weak corrections with those published in [7].

In the second part of the section, we show the predictions for NLO EW RCs obtained by the **SANC** program.

If not specified separately, the following set of input parameters is used:

$$\begin{aligned}
\alpha^{-1}(0) &= 137.035999084 \\
M_W &= 80.379 \text{ GeV} & \Gamma_W &= 2.0836 \text{ GeV} \\
M_Z &= 91.1876 \text{ GeV} & \Gamma_Z &= 2.4952 \text{ GeV} \\
M_H &= 125.0 \text{ GeV} & m_e &= 0.51099895000 \text{ MeV} \\
m_\mu &= 0.1056583745 \text{ GeV} & m_\tau &= 1.77686 \text{ GeV} \\
m_d &= 0.083 \text{ GeV} & m_s &= 0.215 \text{ GeV} \\
m_b &= 4.7 \text{ GeV} & m_u &= 0.062 \text{ GeV} \\
m_c &= 1.5 \text{ GeV} & m_t &= 172.76 \text{ GeV}
\end{aligned}$$

with the angular cuts for at least two photons: $|\cos\theta_\gamma| < 0.9$. In practical calculations we used $\Gamma_W = \Gamma_Z = 0$.

3.1 Comparison with other codes

Firstly, we have compared the results for the Born cross section for several c.m. energies ($\sqrt{s} = 250, 500, 1000 \text{ GeV}$) and the degree of initial beam polarization. The agreement in 5 digits was found, so we omitted the corresponding table.

Secondly, we have compared the results for the hard photon bremsstrahlung cross section for the same c.m. energies with the **CalcHEP** and **WHIZARD** codes. The results are given within the $\alpha(0)$ EW scheme in Table 1. For the cross sections, an additional cut on the photon energy $E_\gamma \geq \omega = 10^{-4}\sqrt{s}/2$ is applied. At least two photons lie in $|\cos\theta_\gamma| < 0.9$. The comparison demonstrates very good (within four to five digits) agreement with the above-mentioned codes

Table 1: The triple tuned comparison between the **SANC** (first line), **CalcHEP** (second line) and **WHIZARD** (third line) results for the hard bremsstrahlung contributions to polarized $e^+e^- \rightarrow \gamma\gamma(\gamma)$ process

$\sqrt{s}, \text{ GeV}$	250	500	1000
SANC	4.467(2)	1.177(1)	0.3095(1)
CalcHEP	4.465(1)	1.177(1)	0.3096(1)
WHIZARD	4.465(1)	1.180(1)	0.3097(1)

We also compared the NLO QED calculations between the **SANC** and **BabaYaga** codes. In Tables 2 and 3, we present a tuned comparison of the integrated cross sections produced for

for two c.m. energy regions: low ($\sqrt{s} = 1$ and 10 GeV) and high ($\sqrt{s} = 91, 160, 240$ and 365 GeV) energies with original setups and cuts (for details, see [7, 28]).

Table 2: The tuned comparison of the Born and NLO QED integrated cross sections produced by the **SANC** and **BabaYaga** codes at low energies

\sqrt{s} , GeV	1	10
Born, nb		
SANC	137.532(1)	1.3755(1)
BabaYaga	137.53	1.3753
NLO QED, nb		
SANC	129.46(2)	1.2623(3)
BabaYaga	129.45	1.2620

Table 3: Tuned comparison of the Born and NLO QED integrated cross sections produced by the **SANC** and **BabaYaga** codes at high energies

\sqrt{s} , GeV	91	160	240	365
Born, pb				
SANC	39.822(1)	12.884(1)	5.7252(1)	2.4758(2)
BabaYaga	39.821	12.881	5.7250	2.4752
NLO QED, pb				
SANC	41.04(1)	13.289(3)	5.907(1)	2.556(1)
BabaYaga	41.043	13.291	5.9120	2.5581

Tables 2 and 3 show perfect agreement of the NLO QED results (within the statistical errors) and we consider these corrections are under control.

To compare the weak part of the NLO RCs, we have produced energy and angular distributions of the relative corrections

$$\delta = \sigma^{\text{1-loop}} / \sigma^{\text{Born}} - 1, \%$$

which are presented in Fig. 1. In the upper panel, the separate contributions for virtual Z and W boson contributions and their sum are shown as a function of unpolarized beams. In the lower panel the angular distributions for several c.m. energies are given.

The obtained RCs show very good qualitative agreement with those given in Fig. 3 of [7].

3.2 Born, one-loop cross sections and relative corrections

In this part of the section, we give our results for the Born, one-loop cross sections and relative corrections ¹. They were calculated with the parameters (3) and the following set of

¹We investigate the energy range 250 – 1000 GeV, because the ILC collider was originally proposed to run at a cms energy $\sqrt{s} = 500$ GeV [29], and recent scenarios with $\sqrt{s} = 250$ GeV and $\sqrt{s} = 1$ TeV [30, 31] were also considered.

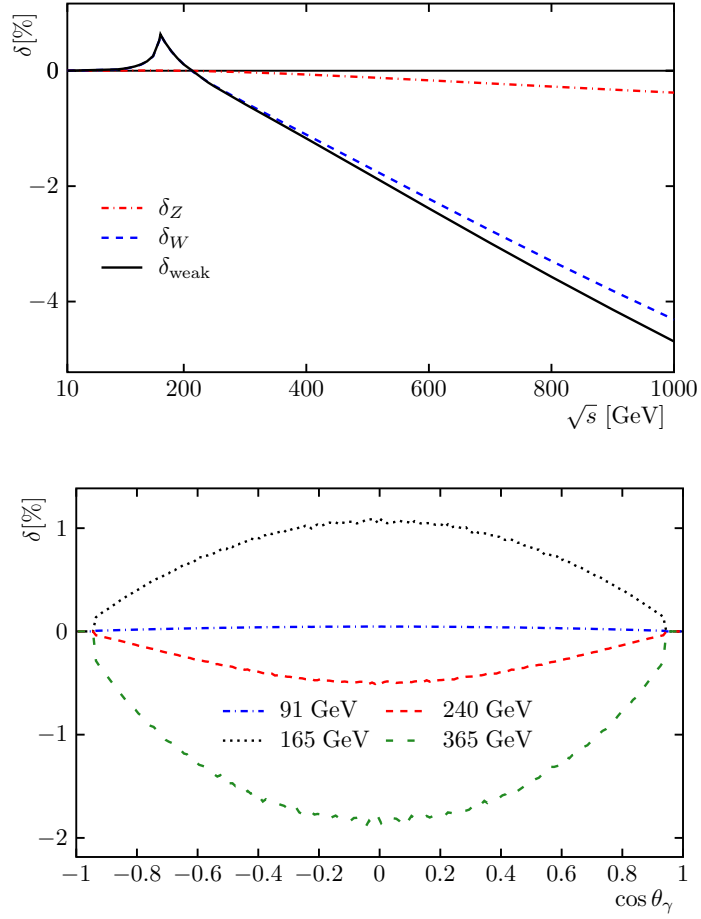


Figure 1: Upper plot: the integrated relative contributions of Z and W bosons to weak RCs. Lower plot: the differential relative weak RCs for c.m. energies at FCCee

the electron (P_{e-}) and positron (P_{e+}) beam polarization:

$$(P_{e-}, P_{e+}) = (0, 0), (0.8, 0.3), (-0.8, 0.3). \quad (16)$$

3.2.1 Energy dependence

In Tables 4 - 6, the results of the integrated Born and one-loop cross sections in pb and the relative corrections in percent are presented separably for NLO QED and weak RC. The results are given for the c.m. energies $\sqrt{s} = 250, 500, 1000$ GeV and for degrees (16) of the initial particle polarization in the $\alpha(0)$ EW scheme.

As it is seen from the tables, the cross sections and the weak RCs are sensitive to the degree of the initial beam polarization while the QED RCs are rather flat. For c.m. energy $\sqrt{s} = 250$ GeV the weak RCs are negative and relatively small compared to QED RCs (approximately 5 – 6 times). As for c.m. energy $\sqrt{s} = 1000$ GeV the weak RCs become compatible with

the QED RCs in the unpolarized case (6.9% vs -5.1%) and even larger (6.9% vs -8.6%) for polarization $(P_{e-}, P_{e+}) = (-0.8, 0.3)$ but with the opposite sign. This means that the weak RCs dominates at high energies and must be taken into account.

Table 4: Born cross section σ (pb), NLO QED and weak relative correction δ (%) for the c.m. energy $\sqrt{s} = 250$ GeV and the set (16) of the polarization degree of the initial particles

P_{e-}, P_{e+}	0, 0	0.8, 0.3	-0.8, 0.3
σ^{Born} , pb	4.2617(1)	3.2388(1)	5.2845(1)
σ^{QED} , pb	4.535(2)	3.4488(5)	5.619(1)
δ^{QED} , %	6.42(4)	6.48(1)	6.32(2)
σ^{weak} , pb	4.2481(1)	3.2345(1)	5.2544(1)
δ^{weak} , %	-0.32(1)	-0.13(1)	-0.57(1)

Table 5: The same as in Tab. 4 but for the c.m. energy $\sqrt{s} = 500$ GeV

P_{e-}, P_{e+}	0, 0	0.8, 0.3	-0.8, 0.3
σ^{Born} , pb	1.06542(1)	0.80972(1)	1.32112(1)
σ^{QED} , pb	1.1365(2)	0.8641(1)	1.4085(3)
δ^{QED} , %	6.67(2)	6.72(2)	6.62(2)
σ^{weak} , pb	1.04396(1)	0.81165(1)	1.25437(1)
δ^{weak} , %	-2.01(1)	0.24(1)	-5.05(1)

Table 6: The same as in Tab. 4 but for the c.m. energy $\sqrt{s} = 1000$ GeV

P_{e-}, P_{e+}	0, 0	0.8, 0.3	-0.8, 0.3
σ^{Born} , pb	0.266353(1)	0.202429(1)	0.330279(1)
σ^{QED} , pb	0.28474(5)	0.21661(4)	0.3531(1)
δ^{QED} , %	6.90(2)	7.00 (2)	6.90(4)
σ^{weak} , pb	0.252650(1)	0.197583(1)	0.301040(1)
δ^{weak} , %	-5.14(1)	-2.39(1)	-8.85(1)

To demonstrate the interference of the QED and weak RCs, we plotted the energy scan. Figure 2 shows the unpolarized QED, weak and summary (EW = QED + weak) relative correction δ (%) for the c.m. energy range $\sqrt{s} = 10 - 1000$ GeV. In the calculations, only angular cuts for at least two photons were applied. As one can see from the picture, the QED RCs dominate in the energy range up to $\sqrt{s} = 100$ GeV. In the range $\sqrt{s} = 100 - 200$ GeV, the weak contribution is positive and increase the NLO RCs. Then the weak relative corrections become negative and start to reduce the total RCs to approximately 2% at $\sqrt{s} = 1000$ GeV. One can see that, the weak corrections change δ_{EW} drastically for high energies (starting approximately from $\sqrt{s} = 200$ GeV). It should also be stressed that additional kinematical cuts such as, for example, photon energy cut, reduce the magnitude of the QED RCs and dominance of the weak RCs becomes harder (stronger?).

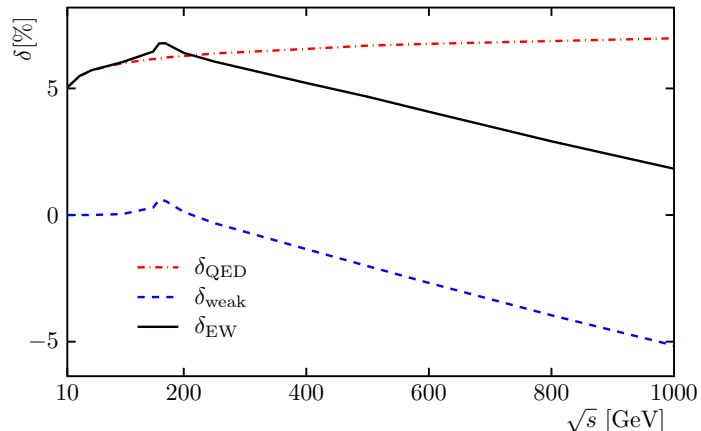


Figure 2: The unpolarized NLO QED, weak and NLO EW relative correction δ (%) for the c.m. energy range $\sqrt{s} = 10 - 1000$ GeV

3.2.2 Left-right asymmetry

The left-right asymmetry is also calculated at c.m. energies $\sqrt{s} = 250, 500, 1000$ GeV, and the angular distributions are shown in Figure 3.

The A_{LR} is defined in the following form:

$$A_{LR} = \frac{\sigma_{LR} - \sigma_{RL}}{\sigma_{LR} + \sigma_{RL}}, \quad (17)$$

where σ_{LR} and σ_{RL} are the cross sections for 100% polarized electron-positron $e_L^- e_R^+$ and $e_R^- e_L^+$ initial states.

As it is seen from the figure, the angular dependence of the asymmetry is very weak at $\sqrt{s} = 250$ GeV but become stronger at $\sqrt{s} = 1000$ GeV. This reaction does not have any clearly seen resonance (in contrast with the s -channel pair-lepton production, for example, where the Z boson defines the peak of the cross section). The asymmetry does not give any experimental information on the mixing angle $\sin^2 \theta_W$ and just shows an order of parity violation.

4 Conclusions and outlook

In this paper, we have considered the complete one-loop electroweak corrections to the process of the polarized electron-positron annihilation into a photon pair within the **SANC** system framework. The helicity amplitudes were used for the Born and virtual parts as well as for the real photon emission (soft/hard bremsstrahlung) taking into account the masses of the initial particles.

The numerical results were evaluated within the **SANC** system framework in the $\alpha(0)$ scheme for c.m. energies from 10 GeV to about 1000 GeV which are relevant for the existing and

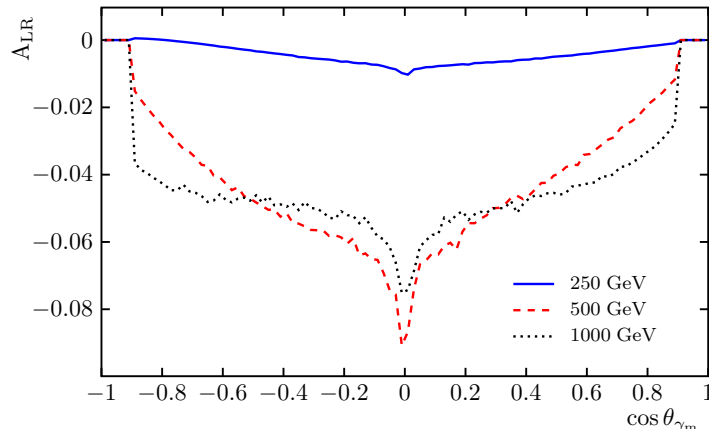


Figure 3: Angular distributions for A_{LR} asymmetry over the highest energy photon angle at several c.m. energies

future e^+e^- colliders. We reached excellent agreement at the tree level for the Born and hard photon bremsstrahlung between **SANC**, **CalcHEP** and **WHIZARD**.

At the one-loop level for unpolarized beams we have compared the obtained results with external codes. Firstly, we performed a tuned comparison of the NLO QED corrections with the **BabaYaga** code and found very good numerical agreement. Secondly, we obtained good qualitative agreement of the weak radiative corrections with the figures given in the world literature.

We have presented the electroweak radiative corrections impacting the Born and complete one-loop cross sections as well as relative corrections at c.m energies $\sqrt{s} = 250, 500, 1000$ GeV. The results are given for unpolarized and polarized cases and demonstrate the strong dependence of the total/differential cross section and relative corrections on the polarization effects.

We would like to emphasize that weak effects give large negative corrections and totally compensate the QED radiative corrections at high energies and therefore must be taken into account.

Analytical calculations for all parts of the cross section were performed for the case of annihilation into vacuum in the massive case $2f2\gamma \rightarrow 0$. This lays the foundation for calculating all cross channels.

Considering the $e^+e^- \rightarrow \gamma\gamma$ process as one for luminometry propose, one needs to take into account high-order effects, such as leading multi-photon QED logarithms and leading two-loop corrections. This is the forthcoming part of our work on this process.

5 Funding

The research is supported by the Russian Science Foundation (project No. 22-12-00021).

References

- [1] FCC Collaboration, A. Abada *et al.*, *Eur. Phys. J.* **C79** (2019), no. 6 474.
- [2] T. Behnke, J. E. Brau, B. Foster, J. Fuster, M. Harrison, J. M. Paterson, M. Peskin, M. Stanitzki, N. Walker, and H. Yamamoto, 1306.6327.
- [3] CEPC Study Group, 1809.00285.
- [4] CEPC Study Group Collaboration, M. Dong *et al.*, 1811.10545.
- [5] M. Aicheler, P. Burrows, M. Draper, T. Garvey, P. Lebrun, K. Peach, N. Phinney, H. Schmickler, D. Schulte, and N. Toge, *A Multi-TeV Linear Collider Based on CLIC Technology: CLIC Conceptual Design Report*. CERN Yellow Reports: Monographs. CERN, Geneva, 2012.
- [6] CEPC Collaboration, I. Smiljanić, I. Božović-Jelisavčić, G. Kačarević, N. Vukašinović, T. Agatonović-Jovin, G. Milutinović-Dumbelović, J. Stevanović, and M. Radulović, “Integrated luminosity measurement at CEPC”, in *International Workshop on Future Linear Colliders*, 5, 2021, 2105.06245.
- [7] C. M. Carloni Calame, M. Chiesa, G. Montagna, O. Nicrosini, and F. Piccinini, *Phys. Lett.* **B798** (2019) 134976, 1906.08056.
- [8] L. M. Brown and R. P. Feynman, *Phys. Rev.* **85** (1952) 231–244, [,120(1952)].
- [9] I. Harris and L. M. Brown, *Phys. Rev.* **105** (1957) 1656–1661.
- [10] F. A. Berends and R. Gastmans, *Nucl. Phys.* **B61** (1973) 414–428.
- [11] S. Eidelman, G. Fedotovitch, E. Kuraev, and A. Sibidanov, *Eur. Phys. J. C* **71** (2011) 1597, 1009.3390.
- [12] C. M. Carloni Calame, H. Czyz, J. Gluza, M. Gunia, G. Montagna, O. Nicrosini, F. Piccinini, T. Riemann, and M. Worek, *Nucl. Phys. Proc. Suppl.* **225-227** (2012) 293–297, 1112.2851.
- [13] C. M. Carloni Calame, “Present Accuracy And Future Prospects Of Monte Carlo Generators For Bhabha And $e^+e^- \rightarrow \gamma\gamma$ ”, in *Mini-Proceedings, 16th meeting of the Working Group on Radiative Corrections and MC Generators for Low Energies*, pp. 5–7, 2014.
- [14] C. M. Carloni Calame, *EPJ Web Conf.* **142** (2017) 01006.
- [15] G. Passarino and M. J. G. Veltman, *Nucl. Phys.* **B160** (1979) 151–207.
- [16] R. Sadykov and V. Yermolchyk, *Comput. Phys. Commun.* **256** (2020) 107445, 2001.10755.

- [17] D. Bardin, Y. Dydyshka, L. Kalinovskaya, L. Rumyantsev, A. Arbuzov, R. Sadykov, and S. Bondarenko, *Phys. Rev. D* **98** (2018), no. 1 013001, 1801.00125.
- [18] S. Bondarenko, Y. Dydyshka, L. Kalinovskaya, L. Rumyantsev, R. Sadykov, and V. Yermolchyk, *Phys. Rev. D* **100** (2019), no. 7 073002, 1812.10965.
- [19] S. Bondarenko, Y. Dydyshka, L. Kalinovskaya, R. Sadykov, and V. Yermolchyk, *Phys. Rev. D* **102** (2020), no. 3 033004, 2005.04748.
- [20] S. G. Bondarenko, L. V. Kalinovskaya, L. A. Rumyantsev, and V. L. Yermolchyk, 2203.10538.
- [21] A. B. Arbuzov, S. G. Bondarenko, L. V. Kalinovskaya, L. A. Rumyantsev, and V. L. Yermolchyk, *Phys. Rev. D* **105** (2022), no. 3 033009, 2112.09361.
- [22] S. Dittmaier, *Phys. Rev.* **D59** (1998) 016007, hep-ph/9805445.
- [23] T. V. Shishkina and V. V. Makarenko, hep-ph/0212409.
- [24] A. Belyaev, N. D. Christensen, and A. Pukhov, *Comput. Phys. Commun.* **184** (2013) 1729–1769, 1207.6082.
- [25] T. Ohl, “WHiZard and O’Mega”, in *Proceedings, LoopFest V: Radiative Corrections for the International Linear Collider: Multi-loops and Multi-legs: SLAC, Menlo Park, California, June 19-21, 2006*, 2006.
- [26] W. Kilian, T. Ohl, and J. Reuter, *Eur. Phys. J.* **C71** (2011) 1742, 0708.4233.
- [27] W. Kilian, S. Brass, T. Ohl, J. Reuter, V. Rothe, P. Stienemeier, and M. Utsch, “New Developments in WHIZARD Version 2.6”, in *International Workshop on Future Linear Collider (LCWS2017) Strasbourg, France, October 23-27, 2017*, 2018, 1801.08034.
- [28] C. M. Carloni Calame, G. Montagna, O. Nicrosini, and F. Piccinini, *EPJ Web Conf.* **218** (2019) 07004.
- [29] P. Bambade *et al.*, 1903.01629.
- [30] K. Fujii *et al.*, 1710.07621.
- [31] CLICdp, ILD concept group Collaboration, A. F. Zarnecki, *PoS CORFU2019* (2020) 037, 2004.14628.